Nickel blended Copper **Ferrite** ($CuNiFe_2O_4$): Synthesis, morphology, supercapacitive features, **and** asymmetric device performance

M. Selvakumar[a], A. Tony Dhiwahar[b], S. Maruthamuthu[c*], Gokul Sidarth Thirunavukkarasu[d], Mehdi Seyedmahmoudian[d], Alex Stojcevski[d], Vasudeva Reddy Minnam Reddy [e] ****

a. Junior scientific officer, Physics Division, Forensic Sciences
b. Department of Physics, Nehru Arts and Science College, Coimbatore, Tamil Nadu, 641105, India
c. PSG Institute of Technology and Applied Research Coimbatore, Tamil Nadu, 641062, India
d. School of Software and Electrical Engineering, Swinburne University of Technology, Melbourne, Australia
e. School of Chemical Engineering, Yeungnam Universit, Gyeongsan, 38541, Republic of Korea

Corresponding author: * smaruthamuthu@gmail.com (S. Maruthamuthu)
Co-corresponding author: ** drmvasudr92@gmail.com (V.R. Minnam Reddy).

Nickel blended Copper **Ferrite** ($CuNiFe_2O_4$): Synthesis, morphology, supercapacitive features, **and** asymmetric device performance

Abstract

Copper ferrite ($CuFe_2O_4$), a cost-effective **and** promising supercapacitive electrode material, **was doped** with highly **electroactive nickel** using a simple microwave combustion process. The presence of **nickel was found to enhance** the electrode kinetics and favours the **fast diffusion process when the material was used to construct a supercapacitor. The nickel blended copper ferrite ($Cu_{0.7}Ni_{0.3}Fe_2O_4$)** exhibited a specific **capacitance of** 1050 Fg^{-1} at a current density of 1 Ag^{-1} in **2 M** KOH electrolyte solution. Further, a reasonable rate of performance and better cyclic stability was observed with the material. **Also, an asymmetric type supercapacitor device was fabricated using $CuNiFe_2O_4$ electrodes, and the electrochemical performance was analyzed.** The fabricated device **showed** an energy density of 21.5 $WhKg^{-1}$ and a power density of 417 WKg^{-1}. These electrochemical **investigations suggest** the potential application of **$Cu_{0.7}Ni_{0.3}Fe_2O_4$** as a supercapacitor electrode material for achieving superior performance.

Keywords: Copper ferrites, microwave combustion, mixed metal **oxides, supercapacitor**

1. Introduction

Supercapacitors (SCs) **are electrochemical** energy storage devices with high power density, long cyclic stability, environmental friendliness, and safety. These exciting properties of SCs find a variety of uses in hybrid electric vehicles, mobile electronic gadgets, and energy backup devices [1, 2]. **Supercapacitor devices** that store electric charge at the electrode and electrolyte solution interface are known **as electric** double-layer capacitors (EDLC). **In contrast, if charge storage occurs due to fast Faradic reactions and electron transfer, the devices are commonly known as pseudocapacitors. Electric double-layer capacitors generally utilize**

carbonaceous materials having high specific area such as, activated carbon, carbon nanotubes, and graphene [3]. **Transition** metal oxides (TMOs), conducting polymers (CPs), and other hybrid electrodes are used as SC electrodes **due to their** multiple transition states and capacity of providing higher capacitance [4-6]. However, in comparison with batteries, SCs may provide higher power density, **but they fail** to facilitate higher energy density. Therefore, the design of SCs with higher energy density is **essential for future technology**. Among different TMOs, Fe_2O_3 is an **attractive material** that can easily blend with divalent metal oxides and form MFe_2O_4. Here, the spinel TMOs (AB_2O_4) having two metal moieties may provide space to design different nanostructures by **varying the metal** composition. Many ferrite structures **have been** fabricated and exploited for SC electrode applications, including $NiFe_2O_4$, $CuFe_2O_4$, $CoFe_2O_4$, and $MnFe_2O_4$ [7-10].

Among these ferrites, copper ferrite ($CuFe_2O_4$)**,** having a unique electronic configuration ($3d^{10}$ $4s^1$) in valance shell**,** makes it favourable for many applications including catalysis, and energy storage [**11, 12**]. Also, it is interesting that nickel ferrite **is a low-cost and environmentally friendly material possessing a high theoretical capacitance and good redox behaviour. In $NiFe_2O_4$, Ni^{2+} ions occupy the octahedral sites, while Fe^{3+} ions occupy both octahedral and tetrahedral sites [13, 14**]. Considering these merits, **introducing copper and nickel in ferrites** is expected to provide enhanced electrochemical behaviour. The energy storage systems commonly use lithium-ion batteries for **distributed renewable energy integrated microgrid** systems and electric vehicles. With the introduction of **superconductor**-based storage systems, the adverse environmental impact of lithium-ion batteries is envisioned to be drastically reduced. Majeed et al. developed a metal-organic framework that advocates the use of **nickel blended copper ferrite ($Cu_{1-x}Ni_xFe_2O_4$)** for large-scale lithium storage applications [15]. The **core-shell** structure of nickel blended copper ferrites **facilitates their** use as anode materials of **high-power lithium-ion** batteries with an

increased rate of performance, adequate AC impedance measurement, cyclic durability with enhanced cyclic performance, **stability, and ultra-fast charging of the storage systems. These properties make nickel blended** copper ferrites an ideal alternative for the energy storage applications. Many blending strategies **such as, precipitation, mechanical milling, hydrothermal method, sol-gel method, combustion, and reverse micelle technique,** are adopted to synthesize **ferrites** [16]. Notably, these methods consume a long synthesis time and draw a lower yield of the samples. Adopting these methods for large-scale industrial applications is difficult [17]. Microwave combustion is an efficient **strategy due to the short time required for sample preparation, rapid reaction rate, and environmentally benign nature.** Further, the microwave method also provides homogeneous and controllable **heating.** The overall efficiency of any SC system relies not only on the electrode materials but also on the electrolyte. In the present scenario, the **abundance of lithium** is depleted due to its excessive use in different kinds of battery systems. Therefore, it is essential to identify specific suitable **alternate ions that can replace lithium.** In this context, an alkaline potassium hydroxide (KOH) electrolyte solution is a good choice due to its higher ionic conductivity, good electrochemical stability, and better solubility in water. In addition, **OH^- ions have** higher mobility in water. Apart from all these advantages, KOH electrolyte is a low-cost material compared to organic and ionic liquid electrolytes making the proposed **nickel** blended copper ferrite a low-cost SC system with increased efficiency.

Reflecting on the points mentioned above, **an attempt has been made** to synthesize Ni-doped copper ferrite **using low-cost precursors by microwave combustion.** The presence of Ni with $CuFe_2O_4$ significantly enhances the supercapacitive features of this doped material. This composite material revealed larger capacitance, good rate performance, and better cyclic stability than the bare $CuFe_2O_4$ sample in **2 M** KOH electrolyte. Further, an asymmetric SC

device (2 electrodes) using Ni-doped $CuFe_2O_4$ and **a high surface area carbon has been fabricated and its performance has been investigated.**

2. Experimental

2.1. Fabrication of $Cu_{0.7}Ni_{0.3}Fe_2O_4$ sample

Analytical grade chemical reagents with high purity such as copper nitrate (Cu $(NO_3)_2.3H_2O$), ferric nitrate ($Fe(NO_3)_3.9H_2O$, nickel nitrate ($Ni(NO_3)_2$), and L-arginine ($C_6H_{14}N_4O_2$) **purchased from Merck, India ,were used as starting materials for the synthesis of the samples. The $Cu_{0.7}Ni_{0.3}Fe_2O_4$ sample was** synthesized using a simple microwave combustion technique. **Briefly, 0.169** g of (Cu $(NO_3)_2.3H_2O$), 0.703 g of (Ni $(NO_3)_2$), 0.808 g of ($Fe(NO_3)_3.9H_2O$, **and the fuel** $C_6H_{14}N_4O_2$ (0.266 g) were **dissolved** in 35 mL of double-distilled water (DDW) maintaining the ratio between fuel and oxidizer as one. The solution was magnetically stirred for **an** hour, and the solution was transferred to a silica crucible carefully. Then, the solution was kept in a microwave system (800 W, CE1041DFB/XTL, and 2.54 GHz frequency) for 10 minutes. After the combustion process, the samples were removed from the oven and annealed at **500°C** for two hours. For the preparation of bare copper ferrite, the same procedure was adopted without using Ni source. The nanoparticles of $CuFe_2O_4$ and $Cu_{0.7}Ni_{0.3}Fe_2O_4$ were labelled as CF and NCF respectively. **The synthesis protocol of $Cu_{0.7}Ni_{0.3}Fe_2O_4$ is shown in Scheme 1.**

Scheme 1. Illustration of the formation of **$Cu_{0.7}Ni_{0.3}Fe_2O_4$.**

*2.2. Analytical **instruments used***

The crystallinity of the samples **was** investigated by a RIGAKU **powder X-ray diffractometer** (CuKα, λ = 1.5418 Å) **between 2θ range from 20 to 90°.** The FT-IR **spectra** of the prepared samples were recorded on **a Nicolet iS10 spectrometer**. The morphological investigations were carried out **using a JEOL** 6360 High-resolution Scanning Electron Microscope system attached with EDX.

2.3. Electrochemical analysis

An electrochemical workstation (CHI 660C, CH Instruments Inc., USA) was used to perform all **the** electrochemical measurements using a 3-electrode setup. The **prepared CF, and NCF** samples were used as working electrodes. A platinum wire and a silver (Ag)/silver chloride (AgCl) were employed as **counter- and reference electrodes, respectively.** Here, the working electrode consists of 85 wt% of the sample, 10 wt% carbon black (Super-P), and 5 wt% polytetrafluoroethylene (PTFE) **(binding material).** Ethanol **was** used as a solvent for preparing the slurry. This slurry mixture was firmly coated over a pre-cleaned current collector (nickel foam, 1 cm^2) and dried at 60**°C** for two hours. Before coating the active material, Ni foam current collectors **were** cleaned using HCl (37 wt%) to remove the impurities on the surface. Additionally, the Ni foam was also cleaned using ethanol and DDW. The prepared electrodes **were** then analyzed using cyclic voltammetry, **charge-discharge measurements, and** impedance measurements **in 2 M KOH** liquid electrolyte. The **supercapacitive features were calculated using the** active electrode mass (0.8 mg).

2.4. Assembly of asymmetric supercapacitor device

A supercapacitor device in asymmetric form using **NCF** and **activated carbon purchased from Sigma-Aldrich (1100 m^2/g)** as positive and negative electrodes **was** fabricated. Analysis of the device was done by using polypropylene **as the** separator and **2 M**

KOH **as the** electrolyte. The equations **used** to evaluate the electrochemical parameters are presented in the supporting information.

3. Results and discussion

3.1 Morphological and structural analysis

The crystallographic information of the prepared samples was investigated using the X-ray diffraction technique. Figure 1a illustrates the diffraction pattern of the CF and NCF samples. The prominent peaks matched well with the JCPDS 77-0010, indicating the formation of copper ferrite (**Fd-3m** space group) with a cubic spinel structure.

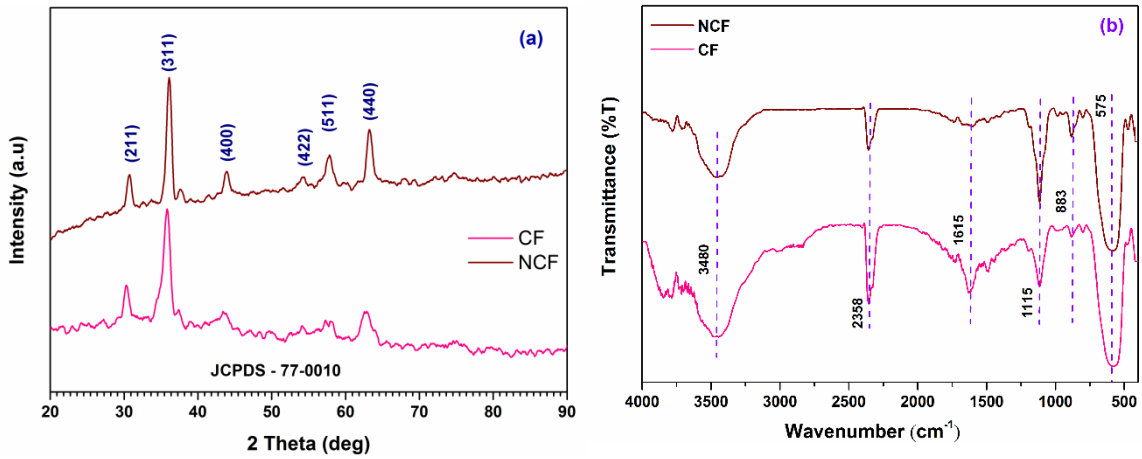

Fig. 1 (a) XRD **spectra** of bare CF and NCF samples. **(b)** FT-IR **spectra** of bare CF and NCF samples

It is to be noted that there is a peak shift (Fig. S1) in **2θ** from 35.80 to 36.15 for the NCF sample. This change in the peak position is attributed to the addition of Ni [18]. The same trend was observed by Nguyen **Kim et al. [19].** To further **understand this peak shift and the effect of Ni on** the CF sample, the crystallite sizes were estimated by **Debye-Scherrer equation** (Supporting information). The estimated crystallite sizes **of** CF and NCF samples **were** 19.3 and 21.8 **nm**, respectively. This increase in **crystallite size indicates the addition of Ni into CF.**

The FTIR spectra of CF and NCF are presented in Fig 1b. In both the spectra, the peak at 575 cm^{-1} is attributed to stretching vibration of Fe^{3+}– O_2 **(tetrahedral voids)** [20]. The band at 883 cm^{-1} is due to spinel **formation** and Cu–O vibration [21]. A sharp peak at 1115 cm^{-1} indicates O–H stretching due to H_2O adsorption [21]. The bands at 2357 cm^{-1} and 1615 cm^{-1} are assigned to CO_2 and bending vibrations of H–O–H [22, 23]. A broad peak observed at 3480 cm^{-1} is attributed to O–H stretching vibrations in H_2O molecules [24].

High resolution SEM images **of** CF and NCF are presented in Fig. 2 (a,b,d,e). The SEM images of both **the** samples exhibit nano-sized particle structure with agglomeration. The **microwave heat and the inter-molecular friction led to particle agglomeration** [24]. To further confirm the presence of Ni in the sample, EDX **analysis was performed.**

3.2 Electrochemical analysis

The supercapacitive features of the synthesized samples were studied by cyclic voltammetry (CV) in the potential window 0-0.5 mVs^{-1}. **Figure** 3 (a) presents the CV curves of CF and NCF electrodes at the voltage sweep rate of 5 mVs^{-1}. The CV curves possess better visible anodic and cathodic peaks indicating the significant influence of redox reaction due to insertion/desertion of electrolyte ions. Also, it is valid to mention that the Ni-blended sample has a large loop area and higher current response. This increased current **in the** NCF **sample is** attributed to electrochemically active Ni **ions** in the sample, which **lower** the internal resistance and **favour** enhanced supercapacitive properties. **Further, Fig.** S3 (a,b) displays CV curves of CF and NCF electrodes at different voltage sweep rates from 5 -100 mVs^{-1}. The increment in the scan rate shifts the anodic and cathodic peaks to lower (or) higher potentials **due to the limitations of the ion diffusion rate to satisfy electronic neutralization during the redox process** [25].

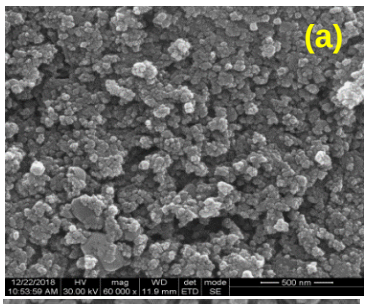

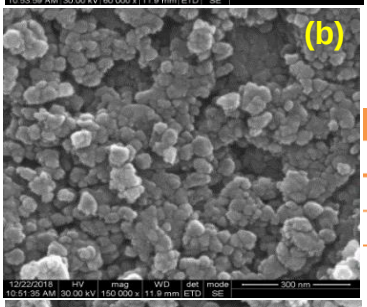

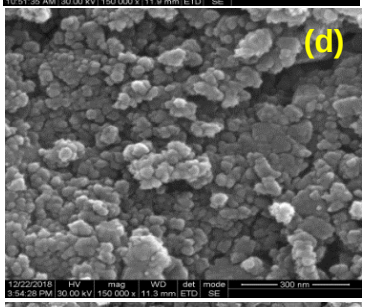

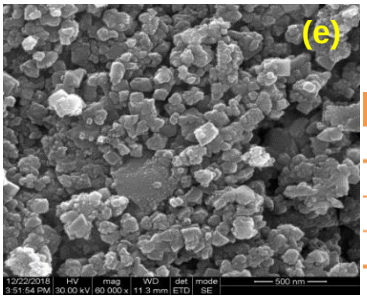

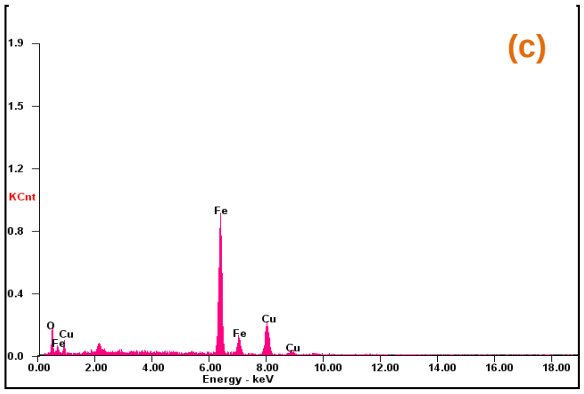

Element	Wt%	At%
OK	14.77	38.64
FeK	57.35	42.99
CuK	27.88	18.37
Matrix	Correction	ZAF

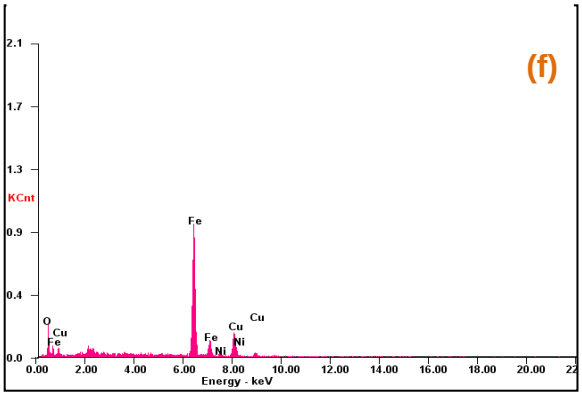

Element	Wt%	At%
OK	17.32	43.11
FeK	57.17	40.77
NiK	02.58	01.75
CuK	22.94	14.37
Matrix	Correction	ZAF

Fig. 2 (a,b & d,e) SEM images of CF and NCF samples. Fig. 2 (c) EDX spectra of sample CF indicating Fe, Cu, and O in the sample. In addition, Fig. 2(f) displaying the EDX spectra of the NCF sample

Galvanostatic discharge measurements (GCD) **were investigated** to understand the charge storage property of the prepared samples. **The GCD** profiles of CF and NCF samples at a current density of 1 Ag^{-1} between the **potentials** 0-0.4 V are presented in Fig 3(b). The nonlinear GCD profiles highlight the influence of redox reactions over the EDLC behaviour of the samples.

The calculated specific capacitance for CF and NCF samples are 620 Fg^{-1} and 1050 $Fg^{-1,}$ respectively. This capacitance value is higher than many reports based on ferrites. For example, ($CuFe_2O_4$-Graphene, 576.6 @ 1 Ag^{-1}), ($CuFe_2O_4$, 334 @ 0.6 Ag^{-1}), ($CuFe_2O_4$, 28 @ 0.5 Ag^{-1}) ,($NiFe_2O_4$/rGO, 584.63 Fg^{-1}@ 1Ag^{-1}), ($NiFe_2O_4$, 168.5 Fg^{-1}@ 1 Ag^{-1}), ($Ni_{1-x}Cu_xFe_2O_4$, 735@ 1.47 m Ag^{-1}), ($CoFe_2O_4$/rGO, 835.7 Fg^{-1}@ 1Ag^{-1}), ($CoFe_2O_4$/MWCNT, 390 F g^{-1} @ 1 mA cm^{-2}), ($CoFe_2O_4$, 503 F g^{-1} @ 1Ag^{-1}) [25-33]. Interestingly, the Ni-doped sample exhibits notably enhanced capacitance due to electroactive Ni in the doped sample. Fig. S3 (c, d) shows the GCD curves of CF and NCF samples at different current densities. The balanced GCD curves at the lower and higher current rates indicate **the ion intercalation and deintercalation process of the Ni-doped SC.**

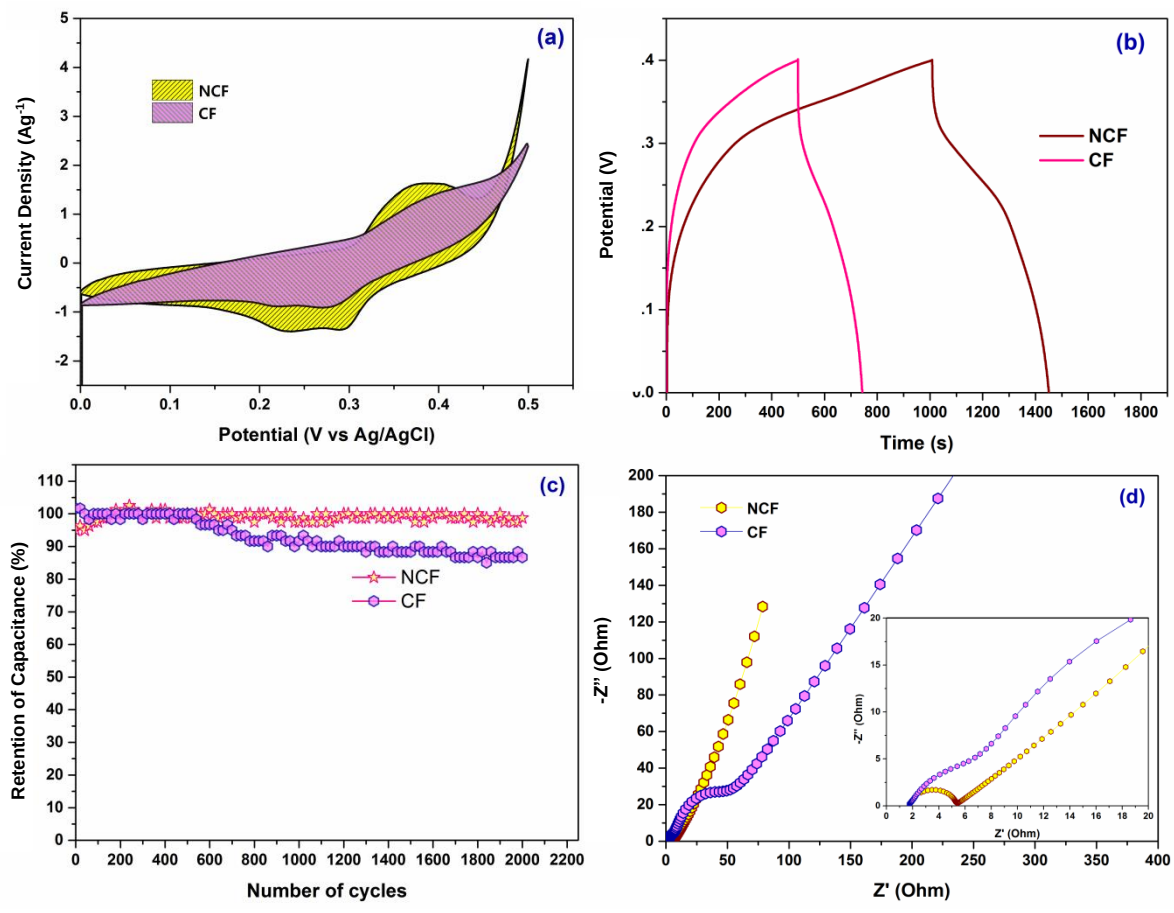

Fig. 3 (a) CV curves of CF and NCF electrodes at a scan rate of 5mVs^{-1}.(b) GCD profiles of CF and NCF electrodes at a current rate of 1Ag^{-1}.(c) Cyclic stability plot for CF and NCF electrodes. (d) Nyquist plot for CF and NCF electrodes (inset presents enlarged image).

Fig. S(3) displays the variation of specific capacitance with various current densities. At lower current rates, electrolyte ions will have sufficient time to access the inner active sites of the electrode, providing larger capacitance. In contrast, the ions get significantly less time for intercalation at higher current rates, leading to lower capacitance [35]. Here, the NCF electrode holds 70% of initial capacitance at 6 Ag^{-1} and 55% capacitance at 8 Ag^{-1}. This capacitance withstanding ability at higher current **reveals** better rate performance of the NCF electrode.

For commercial adaptability of any SC, the **electrode material should have good cyclic stability**. To get better insight into the stability of CF and NCF electrodes, **repeated charge-discharge up to 2000 cycles at a current density of 10 Ag^{-1} was performed,** and the respective plot is presented in Fig. 3c. The NCF electrode holds 98 % of initial capacitance, which is higher than the CF electrode (86%) after 2000 cycles. This result is comparable with some of the literature reports. For instance, $NiFe_2O_4$/rGO (91% after 2000 cycles) [29], $Ni_{1-x}Cu_xFe_2O_4$, (65% after 1000 cycles) [31], $CoFe_2O_4$/MWCNT (91% after 2000 cycles) [33], $CuFe_2O_4$ (90.2% after 1000 cycles) [36],

Electrochemical impedance spectra (EIS) measurements are a better analytical procedure to **study the** resistive and capacitive properties of any SC electrode material. **The EIS investigations for CF and NCF electrodes were performed, and the** Nyquist graph is displayed in Fig 3(d). A circuit used to fix the EIS data is shown in Fig S4. The circuit has charge transfer resistance (R_{CT}), mass capacitance (C_L), double layer capacitance (D_{DL}), and Warburg element (W). An intercept semicircle at the x-axis indicates R_{CT} from ion interfacing at the electrode [37]. The measured R_{CT} values of CF and NCF electrodes are 49 Ω and 3.9 Ω. It is significant to note that the Ni blended sample shows **a minimum** charge transfer resistance compared to the undoped sample. This lower charge transfer resistance is the primary reason

for higher **capacitance and better electrochemical behaviour of NCF. A lower R_{CT} will facilitate better charge-discharge performance** at higher current densities.

3.3 Asymmetric supercapacitor performance

Generally, electrochemical investigation with a two-electrode setup is more reliable for testing the adaptability of the prepared sample for commercial applications. In this view, an asymmetric SC device using NCF and **high surface area activated carbon (AC)** was fabricated. **A polypropylene sheet was used as a separator with 2 M KOH electrolyte.**

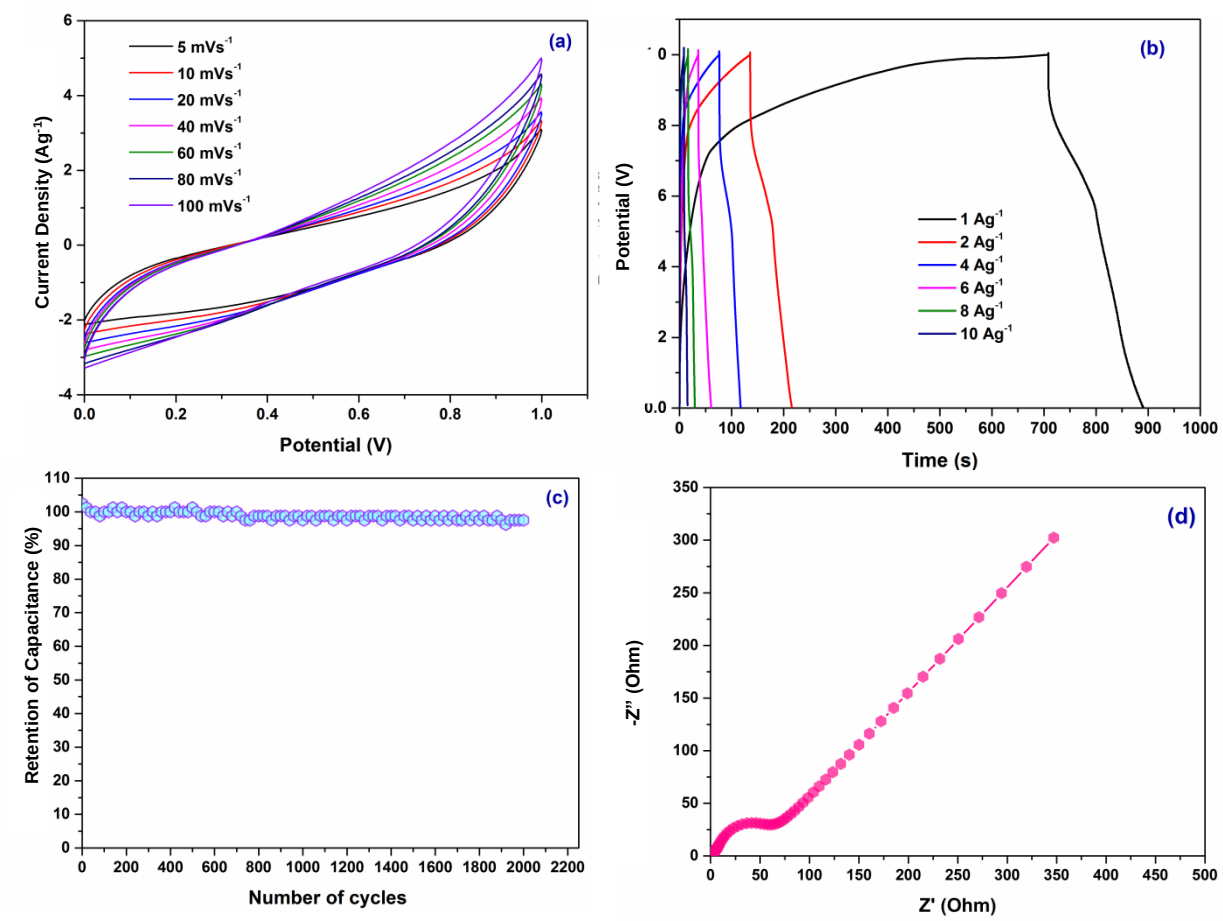

Fig. 4 (a) CV curves of CF//AC device at different voltage. (b) GCD profiles NCF NCF//AC at different current densities. (c) Stability plot for NCF//AC device. (d) Nyquist plot for NCF//AC device

Fig 4(a) shows the CV curves of NCF// AC asymmetric device at different voltage sweep rates from 5 -100 mVs^{-1} **in** the potential window 0-1 V. **The quasi-rectangular shape**

of the curves was found to be maintained at all scan rates. It shows the better reversibility of the device and good capacitive behavior. To estimate the electrochemical parameters of this device, the capacitance, energy, and power densities were evaluated. **The GCD** measurements were carried out for this device at different current densities (1-10 Ag^{-1}). The calculated specific capacitances of this device are 155, 136, 133, 125, 93, and 91 Fg^{-1} at current densities of 1, 2, 4, 6, 8, and 10 Ag^{-1}, **respectively**. **Cyclic** stability is yet another critical parameter that determines the overall efficiency of the supercapacitor device. The cyclic stability investigation for this device (Fig. 4c) was performed up to 2000 repeated charge-discharge cycles at a current rate of 10 Ag^{-1}. This device holds 98% of capacitance after 2000 cycles.

The EIS investigations for this two-electrode cell and Nyquist graph are displayed in Fig 4(d). This device shows an R_{CT} value of 71 Ω, higher than the R_{CT} value measured in the three-electrode cell setup. It is due to the use of additional electrodes with increased total electrode active mass. **Here, the activated carbon** also will contribute to the overall resistance leading higher R_{CT} value for the device. **Further, energy** and power density values are critical aspects for any SC device. **The** values are derived from GCD investigations at a current rate of 1 Ag^{-1}. This two-electrode SC device shows an energy density of 21.5 $WhKg^{-1}$ and a power density of 417 WKg^{-1}. This energy density and power density values are slightly greater than these values reported in literature. **For example, device SC-CoFe33-5: energy density 46.8 $WhKg^{-1}$, power density 34 WKg^{-1}[32], device $Al_{0.2}Cu_{0.4}Co_{0.4}Fe_2O_4$: energy density 3.84 $WhKg^{-1}$, power density 270 WKg^{-1} [38], device $Cu_xMn_{(1-x)}Fe2O4$: power density 386 WKg^{-1}[39], device$(CF)_{0.75}(GNPs)_{0.}$25: energy density 6.49 $WhKg^{-1}$, power density 62.5 WKg^{-1} [40], device ($CuFe_2O_4$–NR@$NiFe_2O_4$–NS): energy density 72 $WhKg^{-1}$ power density 287 WKg^{-1} [41].** These encouraging results derived from these investigations **would pave** the way for using NCF electrodes for high-performance SC devices.

4. Conclusions

The Ni-blended **copper** ferrite **sample** was prepared using a simple and time-efficient microwave combustion procedure **in this work.** The **structural and morphological** analyses were carried out for NCF and bare **CF samples.** These results motivated us to explore the **usefulness of NCF for SC** electrode applications. When tested as an SC electrode, the NCF sample showed very high capacitance, better rate performance, and good cyclic stability. **Further, an asymmetric type SC device utilizing NCF as the active electrode was fabricated and its performance was studied.** Interestingly, this NCF based device showed an energy density of 21.5 $WhKg^{-1}$ and a power density of 417 WKg^{-1}. These results provide additional insights on Ni-doped copper ferrites towards their **future prospects** in SC devices.

References

[1] W. Kang, L. Zeng, S. Ling, C. Zhang, 3D Printed Supercapacitors toward Trinity Excellence in Kinetics, Energy Density, and Flexibility, Advanced Energy Materials 11 (2021) 2100020

[2] B. Saravanakumar, K. K. Purushothaman, G. Muralidharan, ACS Applied Materials & Interfaces 4 (2012) 4484- 4490

[3] R. Liu, A. Zhou, X. Zhang, J. Mu, H. Che, Y. Wang, T. Wang, Z. Zhang, Z. Kou, Fundamentals, Advances and Challenges of Transition Metal Compounds-based Supercapacitors, Chemical Engineering Journal 412 (2021) 128611

[4] Q. Guo, J. Yuan, Y. Tang, C. Song, D. Wang, Self-assembled PANI/CeO_2/$Ni(OH)_2$ hierarchical hybrid spheres with improved energy storage, Electrochimica Acta 367 (2021) 137525

[5] S.H. Lee, J. Lee, J. Jung, A.R. Cho, J.R. Jeong, C.D. Van, J. Nah, M.H. Le, Enhanced Electrochemical Performance of Micro-Supercapacitors Via Laser-Scribed Cobalt/Reduced Graphene Oxide Hybrids, ACS Applied Materials & Interfaces 2021, 13, 16, 18821–18828

[6] B. Asbani, K. Robert, P. Roussel, T. Brousse, C. Lethien, Asymmetric micro-supercapacitors based on electrodeposited Ruo_2 and sputtered VN films, Energy Storage Materials 37 (2021) 207-214

[7] M. Fu, Z. Zhu, Q. Zhuang, Z. Zhang, W. Chen, Q. Liu, In situ growth of manganese ferrite nanorods on graphene for supercapacitors, Ceramics International 46 (2020) 28200-28205

[8] V. Sharma, U.N. Pan, T. Ibomcha Singh, A.K. Das, N.H. Kim, J.H. Lee, Pragmatically designed tetragonal copper ferrite super-architectures as advanced multifunctional electrodes for solid-state supercapacitors and overall water splitting, Chemical Engineering Journal 415 (2021) 127779

[9] M.M. Mumtaz, Nanocomposites of multi-walled carbon nanotubes/cobalt ferrite Nanoparticles: Synthesis, structural, dielectric and impedance spectroscopy, Journal of Alloys and Compounds 866 (2021) 158750

[10] E. Samuel, A. Aldalbahi, M. El-Newehy, H. El-Hamshary, S.S. Yoon, Nickel ferrite beehive-like nanosheets for binder-free and high-energy-storage supercapacitor electrodes, Journal of Alloys and Compounds 852 (2021) 156929

[11] B. Li, M. Li, C. Yao, Y. Shi, D. Ye, J. Wu, D. Zhao, A facile strategy for the preparation of well-dispersed bimetal oxide $CuFe_2O_4$ nanoparticles supported on mesoporous silica, Journal of Materials Chemistry A 1 (2013) 6742–6749.

[12] D. Wang, D. Astruc, Fast-growing field of magnetically recyclable nanocatalysts, Chemical Reviews 114 (2014) 6949–6985

[13] X. Wang, L. Yu, X. Wu, F. Yuan, Y. Guo, Y. Ma, J. Yao, Synthesis of single-crystalline Co_3O_4 octahedral cages with tunable surface aperture and their lithium storage properties, The Journal of Physical Chemistry C 113 (2009) 15553-15558.

[14] S. Anwar, K.S. Muthu, V. Ganesh, N. Lakshminarasimhan, A comparative study of electrochemical capacitive behavior of NiFe2O4 synthesized by different routes, Journal of the Electrochemical Society158 (2011) A976-A981.

[15] Majeed, M.K., Saleem, A., Majeed, M.U., Lotfi, M., Hussain, M.M. and Gong, H., 2021. Metal–organic framework mediated nickel doped copper ferrite for superior lithium storage. Sustainable Energy & Fuels.

[16] A. Manikandan, J. Judith Vijaya, L. John Kennedy, M. Bououdina, Structural, optical and magnetic properties of $Zn_{1-x}Cu_xFe_2O_4$ nanoparticles prepared by microwave combustion method, Journal of Molecular Structure 1035 (2013), 332-340

[17] A. Manikandan, J. Judith Vijaya, M.Sundararajan, C.Meganathan, L. JohnKennedy, M. Bououdina, Optical and magnetic properties of Mg-doped $ZnFe_2O_4$ nanoparticles prepared by rapid microwave combustion method, Superlattices and Microstructures 64 (2013) 118-131

[18] A. Tony Dhiwahar, M. Sundararajan, P. Sakthivel, C.S. Dash, S. Yuvaraj, Microwave-assisted combustion synthesis of pure and zinc-doped copper ferrite nanoparticles: structural,

morphological, optical, vibrational, and magnetic behavior, Journal of Physics and Chemistry of Solids 138 (2020) 109257

[19] N.K. Thanh, T.T. Loan, L.N. Anh, N.P. Duong, S. Soontaranon, N. Thammajak, T. Duc Hien, Cation distribution in $CuFe_2O_4$ nanoparticles: effects of Ni doping on magnetic properties, Journal of Applied Physics120 (2016) 142115.

[20] S. Moortheswaran, A. Manikandan, S. Sujatha, S.K. Jaganathan, S.A. Antony, One-pot combustion synthesis and characterization studies of spinel $CoAl_2O_4$ nano-catalysts, Nanoscience and Nanotechnology Letters 8 (2016) 424–427.

[21] Z. Chen, Y. Yan, J. Liu, Y. Yin, H. Wen, J. Zao, D. Liu, H. Tian, C. Zhang, S. Li, Microwave induced solution combustion synthesis of nano-sized phosphors, Journal of Alloys and Compounds 473 (2009) L13–L16.

[22] B. Saravanakumar , C. Radhakrishnan , Murugan Ramasamy ,Rajendran Kaliaperumal, Allen J. Britten, M. Mkandawire, Copper oxide/mesoporous carbon nanocomposite synthesis, morphology and electrochemical properties for gel polymer-based asymmetric supercapacitors, Journal of Electroanalytical Chemistry 852 (2019) 113504-113515

[23] H. Mohebbi, T. Ebadzadeh, F.A. Hesari, Synthesis of nano-crystalline NiO-YSZ by microwave-assisted combustion synthesis, Powder Technology188 (2009) 183–186.

[24] M.A. Rehman, I. Yusoff, Y. Alias, Fluoride adsorption by doped and un-doped magnetic ferrites $CuCe_xFe_{2-x}O4$: preparation, characterization, optimization and modeling for effectual remediation technologies, Journal of Hazardous Materials 299 (2015) 316–324

[25] K. K. Purushothaman , I. M. Babu, B. Saravanakumar, Hierarchical mesoporous $Co_x Ni_{1-x}O$ as advanced electrode material for hybrid supercapacitors, International journal of hydrogen energy 42 (2017) 28445- 28452

[26] W. Zhang, B Quan, C. Lee, S. K. Park, X. Li, E. Choi, G. Diao, Y. Piao, One-Step Facile Solvothermal Synthesis of Copper Ferrite−Graphene Composite as a High-Performance Supercapacitor Material Applied Surface Science 7 (2015) 2404−2414

[27] S. Giri, D. Ghosh, A. P. Kharitonov, C. K. Das, Study of Copper Ferrite Nanowire Formation in Presence of Carbon Nanotubes and Influence of Fluorination on High Performance Supercapacitor Energy Storage Application, Functional Materials Letters 5 (2012) 1250046

[28] J. Zhao, Y. Chessng, X. Yan, D. Sun, F. Zhu, Q Xue, Magnetic and Electrochemical Properties of $CuFe_2O_4$ Hollow Fibers Fabricated by Simple Electrospinning and Direct Annealing. Cryst Eng Comm 14 (2012) 5879−5885

[29] M. B. Askari, P. Salarizadeh, Binary nickel ferrite oxide ($NiFe_2O_4$) nanoparticles coated on reduced graphene oxide as stable and high-performance asymmetric supercapacitor electrode material, International Journal of Hydrogen Energy 45 (2020) 27482-27491

[30] M. Fu, Z. Zhu, Y. Zhou, W. Xu, W. Chen, Q. Liu, X. Zhu , Multifunctional pompon flower-like nickel ferrites as novel pseudocapacitive electrode materials and advanced absorbing materials, Ceramics International 46 (2020) 850-856

[31] B. Bashir, A. Rahman, H. Sabeeh, M. Azhar Khan, M. F.Aly Aboud, M. F. Warsi, I. Shakir, P. O. Agboola, M. Shahid, Copper substituted nickel ferrite nanoparticles anchored onto the graphene sheets as electrode materials for supercapacitors fabrication, Ceramics International 45 (2019) 6759-6766

[32] S. Martinez-Vargas, A.I. Mtz-Enriquez, H. Flores-Zuñiga, A. Encinas, J. Oliva, Enhancing the capacitance and tailoring the discharge times of flexible graphene supercapacitors with cobalt ferrite nanoparticles, Synthetic Metals 264 2020 116384

[33] J. Acharya, B. G. Sundara Raj, T. H. Ko, M. Seob Khil, H. Y. Kim, B.S. Kim , Facile one pot sonochemical synthesis of $CoFe_2O_4$/MWCNTs hybrids with well-dispersed MWCNTs for asymmetric hybrid supercapacitor applications, International Journal of Hydrogen Energy 45 (2020) 3073-3085

[34] H. Gao, J. Xiang, Y. Cao, Hierarchically porous $CoFe_2O_4$ nanosheets supported on Ni foam with excellent electrochemical properties for asymmetric supercapacitors, Applied Surface Science 413 (2017) 351-359

[35] B. Saravanakumar, K.K. Purushothaman, G. Muralidharan, Interconnected V_2O_5 nanoporous network for high-performance supercapacitors, ACS Applied Materials & Interfaces 4 (2012) 484-4490.

[36] M. Khairy, M.G. El-Shaarawy, M.A. Mousa, Characterization and super-capacitive properties of nanocrystalline copper ferrite prepared via green and chemical methods, Materials Science and Engineering B 263 (2021) 114812

[37] D. Antiohos, K. Pingmuang, M.S. Romano, S. Beirne, T. Romeo, P. Aitchison, A. Minett, G. Wallace, S. Phanichphant, J. Chen, Manganositee microwave exfoliated graphene oxide composites for asymmetric supercapacitor device applications, Electrochimica Acta 101 (2013) 99-108

[38] Bhamini Bhujun, Tichelle T.T. Tan, Anandan S. Shanmugam, Evaluation of aluminium doped spinel ferrite electrodes for supercapacitors, Ceramics International 42 (2016) 6457 – 6466

[39] Gita singh and sudeshna Chandra, Copper doped manganese ferrites PANI for fabrication of binder – free nanohybrid symmetrical supercapacitors, Journal of the Electrochemical society, 166(6) A1154-A1159 (2019)

[40] M. Israr, Javed Iqbal, Aqsa Arshad, P. Gomez-Romero, Sheet-on-sheet like calcium ferrite and graphene nanoplatelets nanocomposite: A multifunctional nanocomposite for high-performance supercapacitor and visible light driven photo catalysis, Journal of solid state chemistry 293 (2021) 121646

[41] Shybhangi B. Bandgar, Madagonda M. Vadiyar, Chitra L. Jambhale, Zhibin Ye, Jin-Hyeok Kim, Sanjay S. Kolekar, Construction of dual metal ferrite-based core-shell nanostructures as low-cost multimetal electrode for boosting energy density of flexible asymmetric supercapattery, Journal of energy storage 36 (2021) 102379